

Rotational structures and the wobbling mode in ^{167}Ta

D. J. Hartley,¹ R. V. F. Janssens,² L. L. Riedinger,³ M. A. Riley,⁴ X. Wang,⁴ A. Aguilar,^{4,*} M. P. Carpenter,² C. J. Chiara,^{2,5,6} P. Chowdhury,⁷ I. G. Darby,³ U. Garg,⁸ Q. A. Ijaz,⁹ F. G. Kondev,⁵ S. Lakshmi,⁷ T. Lauritsen,² A. Ludington,¹ W. C. Ma,⁹ E. A. McCutchan,² S. Mukhopadhyay,^{8,†} R. Pifer,¹ E. P. Seyfried,¹ U. Shirwadkar,⁷ I. Stefanescu,^{2,6} S. K. Tandel,^{7,‡} J. R. Vanhoy,¹ S. Zhu,² and S. Frauendorf⁸

¹*Department of Physics, U.S. Naval Academy, Annapolis, Maryland 21402, USA*

²*Physics Division, Argonne National Laboratory, Argonne, Illinois 60439, USA*

³*Department of Physics and Astronomy, University of Tennessee, Knoxville, Tennessee 37996, USA*

⁴*Department of Physics, Florida State University, Tallahassee, Florida 32306, USA*

⁵*Nuclear Engineering Division, Argonne National Laboratory, Argonne, Illinois 60439, USA*

⁶*Department of Chemistry and Biochemistry, University of Maryland, College Park, Maryland 20742, USA*

⁷*Department of Physics, University of Massachusetts Lowell, Lowell, Massachusetts 01854, USA*

⁸*Department of Physics, University of Notre Dame, Notre Dame, Indiana 46556, USA*

⁹*Department of Physics, Mississippi State University, Mississippi State, Mississippi 39762, USA*

(Received 28 March 2011; published 13 June 2011)

Excited states in the neutron-deficient nucleus ^{167}Ta were studied through the $^{120}\text{Sn}(^{51}\text{V},4n)$ reaction. Twelve rotational bands have been observed and the relative excitation energy of each sequence is now known owing to the multiple interband connections. Several quasineutron alignments were observed that aided in the quasiparticle assignments of these bands. The resulting interpretation is in line with observations in neighboring nuclei. Trends in the wobbling phonon energy seen in $^{161,163,165,167}\text{Lu}$ and ^{167}Ta are also discussed and particle-rotor model calculations (assuming constant moments of inertia) are found to be inconsistent with the experimental data.

DOI: [10.1103/PhysRevC.83.064307](https://doi.org/10.1103/PhysRevC.83.064307)

PACS number(s): 21.10.Re, 23.20.Lv, 25.70.Hi, 27.70.+q

I. INTRODUCTION

The wobbling phenomenon associated with triaxial nuclei, first found in ^{163}Lu [1], has drawn considerable interest for nearly a decade. Although this exotic collective mode was first thought to be a general feature of the $Z \approx 72$, $N \approx 94$ region [2], finding examples besides the odd- A lutetium nuclei proved to be challenging to the extent that a recent suggestion was even made that lutetium nuclei might be the only ones suitable for displaying wobbling bands [3]. Hence, it was surprising to find evidence for a wobbling band (which can only occur if the nucleus possesses a stable asymmetric shape) in the nucleus $^{167}\text{Ta}_{94}$ [4]. The predicted $N = 94$ triaxial strongly deformed (TSD) gap [5] responsible for stabilizing asymmetric shapes is well established, as all wobbling bands are observed near this neutron number, but the discovery of the asymmetric shape in ^{167}Ta raises new questions in regards to the role of the proton Fermi surface.

The identification of the ^{167}Ta wobbling band, which feeds into a structure based on a $\pi i_{13/2}$ quasiparticle excitation, was previously discussed in Ref. [4]. The present paper uses the same measurement and addresses the full spectroscopy of ^{167}Ta including an analysis of the band crossings in the 12 rotational sequences and the $B(M1)/B(E2)$ ratios determined for the strongly coupled bands. Quasiparticle assignments

could be confidently proposed to 9 of the 12 structures. In addition, the systematic feature of the wobbling phonon energy decreasing with spin in $^{161,163,165,167}\text{Lu}$ [1,2,6,7] and ^{167}Ta will be discussed. At present, particle-rotor model predictions, assuming constant moments of inertia, cannot reproduce this trend.

II. EXPERIMENTAL DETAILS

High-spin states in ^{167}Ta were populated via the $^{120}\text{Sn}(^{51}\text{V},4n)$ reaction, where the ^{51}V beam was accelerated to an energy of 235 MeV by the ATLAS facility at Argonne National Laboratory. A beam current of 2–2.5 pA was sustained throughout the 5-day experiment. This beam bombarded two stacked, self-supporting ^{120}Sn targets, each having a thickness of $500 \mu\text{g}/\text{cm}^2$. The Gammasphere array [8,9] detected the reaction γ rays with 101 Compton-suppressed detectors, such that approximately 2×10^9 fourfold or greater coincidence events were recorded. A Blue database [10] was constructed from these events to build Radware [11] coincidence cubes and hypercubes, as well as to facilitate angular-correlation measurements used to assign relative spins and parity to the levels.

The angular-correlation analysis was performed by gating on two known $E2$ transitions in the Blue database and projecting the coincident transitions into 16 one-dimensional spectra associated with the 16 rings of Gammasphere. The spectra from the 5 rings nearest 90° ($\theta = 79^\circ, 81^\circ, 90^\circ, 99^\circ$, and 101°) were summed together such that the intensities of the γ rays, $W(\theta_{90^\circ})$, were determined. In a similar manner, the intensities of the transitions from the five most backward rings, $W(\theta_b)$ where $\theta = 122^\circ, 130^\circ, 143^\circ, 148^\circ$, and 163° , were

*Present address: Department of Radiation Oncology, University of Pennsylvania, Philadelphia, Pennsylvania 19104, USA.

†Present address: Nuclear Physics Division, Bhabha Atomic Research Centre, Mumbai 400085, India.

‡Present address: Centre for Excellence in Basic Sciences, Mumbai 400098, India.

TABLE I. Table of spin and parity assignments for states in ^{167}Ta , as well as γ -ray energies, intensities, and angular correlation ratios.

I^π ^a	E_{level} (keV)	E_γ (keV) ^b	I_γ ^c	R_{ang}	Band _{f} , I_f ^d
Band 1: $\pi h_{11/2}[514]9/2 \alpha = +1/2$					
9/2 ⁻	206.4				
13/2 ⁻	496.3	289.9	$\sim 29^f$	0.86(7) ^g	1, 9/2 ⁻
		190.8	$\sim 136^f$	0.81(3)	1, 11/2 ⁻
17/2 ⁻	947.3	451.0	78(5)	0.91(5)	1, 13/2 ⁻
		268.5	112(8)	0.84(4)	1, 15/2 ⁻
21/2 ⁻	1493.3	546.0	69(5)	1.01(5)	1, 17/2 ⁻
		327.7	69(5)	0.83(3)	1, 19/2 ⁻
25/2 ⁻	2096.6	603.3	60(5)	0.78(2)	1, 21/2 ⁻
		364.2	36(3)	0.79(3)	1, 23/2 ⁻
29/2 ⁻	2717.8	621.2	31(3)	1.20(7)	1, 25/2 ⁻
		368.7	21(2)	0.75(3)	1, 27/2 ⁻
33/2 ⁻	3326.4	608.6	24(2)	0.96(4)	1, 29/2 ⁻
		346.8	16(2)	0.64(4)	1, 31/2 ⁻
37/2 ⁻	3913.3	586.9	18(2)	1.21(7) ^g	1, 33/2 ⁻
		318.8	17(1)	0.77(5)	1, 35/2 ⁻
41/2 ⁻	4501.5	588.2	13(1)	1.21(7) ^g	1, 37/2 ⁻
		311.5	12(1)	0.81(5)	1, 39/2 ⁻
45/2 ⁻	5126.9	625.4	11(1)	1.19(10)	1, 41/2 ⁻
		327.0	7.3(7)	0.83(3)	1, 43/2 ⁻
49/2 ⁻	5802.4	675.5	9.2(9)	1.15(13)	1, 45/2 ⁻
		337.4	3.6(5)	0.76(3) ^g	1, 47/2 ⁻
53/2 ⁻	6518.5	716.1	7.1(8)	1.18(10) ^g	1, 49/2 ⁻
		336.4	2.5(4)	0.76(3) ^g	1, 51/2 ⁻
57/2 ⁻	7292.9	774.4	5.4(6)	1.11(12)	1, 53/2 ⁻
		373.3	1.2(2)		1, 55/2 ⁻
61/2 ⁻	8128.3	835.4	4.0(6)	0.82(10)	1, 57/2 ⁻
65/2 ⁻	9020.7	892.4	2.2(3)		1, 61/2 ⁻
69/2 ⁻	9972.8	952.1	1.2(2)		1, 65/2 ⁻
73/2 ⁻	10 986.8	1014.0	0.4(2)		1, 69/2 ⁻
77/2 ⁻	12 065.5	1078.7	<0.3		1, 73/2 ⁻
Band 1: $\pi h_{11/2}[514]9/2 \alpha = -1/2$					
11/2 ⁻	305.5	99.1	$\sim 58^e$	0.75(5)	1, 9/2 ⁻
15/2 ⁻	678.9	373.4	86(5)	0.85(5)	1, 11/2 ⁻
		182.5	86(7)	0.75(4)	1, 13/2 ⁻
19/2 ⁻	1165.7	486.8	97(7)	0.91(5)	1, 15/2 ⁻
		218.2	52(4)	0.82(5)	1, 17/2 ⁻
23/2 ⁻	1732.5	566.8	93(7)	0.93(3)	1, 19/2 ⁻
		239.1	30(3)	0.73(3)	1, 21/2 ⁻
27/2 ⁻	2349.0	616.5	79(4)	1.04(3)	1, 23/2 ⁻
		252.3	21(1)	0.74(4)	1, 25/2 ⁻
31/2 ⁻	2979.6	630.6	54(4)	1.00(5)	1, 27/2 ⁻
		261.8	16(1)	0.77(5)	1, 29/2 ⁻
35/2 ⁻	3594.4	614.8	30(3)	0.96(5)	1, 31/2 ⁻
		268.1	17(2)	0.84(4)	1, 33/2 ⁻
39/2 ⁻	4190.0	595.6	21(2)	0.89(2)	1, 35/2 ⁻
		276.8	16(1)	0.71(5)	1, 37/2 ⁻
43/2 ⁻	4799.9	609.9	15(1)	1.05(6)	1, 39/2 ⁻
		298.5	8.3(8)	0.66(6)	1, 41/2 ⁻
47/2 ⁻	5465.1	665.2	9.4(9)	1.06(8)	1, 43/2 ⁻
		338.3	5.4(6)	0.76(3) ^g	1, 45/2 ⁻
51/2 ⁻	6182.2	717.1	6.7(7)	1.18(10) ^g	1, 47/2 ⁻
		379.8	3.0(4)		1, 49/2 ⁻
		667.2	0.6(1)		4, (47/2 ⁻)
55/2 ⁻	6919.7	737.5	4.0(5)		1, 51/2 ⁻
		401.2	1.5(2)		1, 53/2 ⁻

TABLE I. (Continued.)

I^π ^a	E_{level} (keV)	E_γ (keV) ^b	I_γ ^c	R_{ang}	Band _f , I_f ^d
59/2 ⁻	7716.4	796.7	4.0(5)		1, 55/2 ⁻
		423.5	1.0(2)		1, 57/2 ⁻
63/2 ⁻	8564.3	847.9	2.9(4)		1, 59/2 ⁻
67/2 ⁻	9466.1	901.8	1.4(2)		1, 63/2 ⁻
71/2 ⁻	10 424.3	958.2	0.8(4)		1, 67/2 ⁻
75/2 ⁻	11 434.8	1010.5	0.4(2)		1, 71/2 ⁻
79/2 ⁻	12 492.9	1058.1	<0.3		1, 75/2 ⁻
83/2 ⁻	13 596.3	1103.4	<0.3		1, 79/2 ⁻
Band 2: $\pi h_{11/2} AB \alpha = +1/2$					
25/2 ⁻	2579.7	380.4	15(2)		2a, 21/2 ⁻
		1086.4	33(3)	1.04(6)	1, 21/2 ⁻
		847.2	12(1)	0.54(6)	1, 23/2 ⁻
		483.2	20(2)	1.02(6)	1, 25/2 ⁻
		345.3	3.3(3)		Misc
29/2 ⁻	2753.5	656.9	20(2)	1.04(7)	1, 25/2 ⁻
		101.5	16(1)	0.60(5)	2, 27/2 ⁻
		539.6	14(1)	0.94(3)	3, 25/2 ⁻
		404.4	21(2)	0.89(5)	1, 27/2 ⁻
33/2 ⁻	3041.9	288.4	9(1)	0.86(7) ^g	2, 29/2 ⁻
		167.5	58(5)	0.71(2)	2, 31/2 ⁻
37/2 ⁻	3468.9	427.0	25(2)	0.94(4) ^g	2, 33/2 ⁻
		233.7	63(5)	0.76(2)	2, 35/2 ⁻
41/2 ⁻	4023.6	554.7	45(3)	1.16(5)	2, 37/2 ⁻
		289.8	48(5)	0.77(2)	2, 39/2 ⁻
45/2 ⁻	4684.3	660.7	40(3)	0.98(6)	2, 41/2 ⁻
		336.1	39(3)	0.76(3)	2, 43/2 ⁻
49/2 ⁻	5426.7	742.4	40(3)	1.18(6)	2, 45/2 ⁻
		373.0	27(3)	0.85(5)	2, 47/2 ⁻
53/2 ⁻	6226.5	799.8	32(3)	0.97(5)	2, 49/2 ⁻
		401.7	12(1)	0.70(8)	2, 51/2 ⁻
57/2 ⁻	7064.0	837.5	22(2)	0.86(5)	2, 53/2 ⁻
		426.2	6.7(8)	0.94(4) ^g	2, 55/2 ⁻
61/2 ⁻	7933.7	869.7	12(1)	1.13(8)	2, 57/2 ⁻
		453.1	4.0(5)		2, 59/2 ⁻
65/2 ⁻	8843.8	910.1	7.3(6)	0.99(8)	2, 61/2 ⁻
		489.2	3.6(4)		2, 63/2 ⁻
69/2 ⁻	9805.2	961.4	5.8(6)		2, 65/2 ⁻
73/2 ⁻	10 825.7	1020.5	1.9(2)		2, 69/2 ⁻
77/2 ⁻	11 907.1	1081.4	0.7(3)		2, 73/2 ⁻
81/2 ⁻	13 047.4	1140.3	0.4(2)		2, 77/2 ⁻
85/2 ⁻	14 230.0	1182.6	<0.3		2, 81/2 ⁻
Band 2: $\pi h_{11/2} AB \alpha = -1/2$					
27/2 ⁻	2652.0				
31/2 ⁻	2874.4	222.4	$\sim 4^f$		2, 27/2 ⁻
		120.9	36(4)	0.72(3)	2, 29/2 ⁻
		156.6	3.4(4)		1, 29/2 ⁻
35/2 ⁻	3235.2	360.8	20(2)	1.06(7)	2, 31/2 ⁻
		193.3	59(7)	0.69(2)	2, 33/2 ⁻
39/2 ⁻	3733.7	498.5	32(3)	1.11(4)	2, 35/2 ⁻
		264.9	50(5)	0.73(2)	2, 37/2 ⁻
43/2 ⁻	4348.1	614.4	36(3)	0.96(5)	2, 39/2 ⁻
		324.5	50(5)	0.70(3)	2, 41/2 ⁻
47/2 ⁻	5053.7	705.6	44(4)	1.17(5)	2, 43/2 ⁻
		369.4	31(3)	0.75(3)	2, 45/2 ⁻
51/2 ⁻	5824.9	771.2	36(3)	0.96(7)	2, 47/2 ⁻
		398.2	20(2)	0.74(4)	2, 49/2 ⁻

TABLE I. (*Continued.*)

I^π ^a	E_{level} (keV)	E_γ (keV) ^b	I_γ ^c	R_{ang}	Band _f , I_f ^d
55/2 ⁻	6637.8	812.9	25(3)	1.18(9)	2, 51/2 ⁻
		411.3	9.4(9)		2, 53/2 ⁻
59/2 ⁻	7480.5	842.7	17(2)	0.92(5)	2, 55/2 ⁻
		416.5	6.1(6)		2, 57/2 ⁻
63/2 ⁻	8354.7	874.2	9.6(9)	1.06(9)	2, 59/2 ⁻
		420.9	4.0(4)		2, 61/2 ⁻
67/2 ⁻	9267.5	912.8	7.7(8)	1.02(10)	2, 63/2 ⁻
		423.5	1.2(2)		2, 65/2 ⁻
71/2 ⁻	10 224.2	956.6	5.0(5)		2, 67/2 ⁻
75/2 ⁻	11 225.7	1001.5	2.2(3)		2, 71/2 ⁻
79/2 ⁻	12 271.4	1045.7	0.8(4)		2, 75/2 ⁻
83/2 ⁻	13 358.0	1086.6	0.4(2)		2, 79/2 ⁻
87/2 ⁻	14 483.4	1125.4	<0.3		2, 83/2 ⁻
Band 2a: $\alpha = +1/2$					
13/2 ⁻	1133.5	637.1	2.5(3)		1, 13/2 ⁻
		454.7	1.1(2)		1, 15/2 ⁻
17/2 ⁻	1641.6	508.1	2.5(3)		2a, 13/2 ⁻
		962.7	1.5(2)		1, 15/2 ⁻
		694.2	4.0(5)	1.1(1)	1, 17/2 ⁻
		475.9	3.6(4)		1, 19/2 ⁻
21/2 ⁻	2199.3	557.7	9(1)		2a, 17/2 ⁻
		705.8	6.1(7)		1, 21/2 ⁻
		466.8	5.0(5)	0.81(9)	1, 23/2 ⁻
Band 3: $\pi h_{9/2}[541]1/2 \alpha = +1/2$					
5/2 ⁻	496.8	496.8	$\sim 7^f$	0.72(3)	6, 3/2 ⁺
		263.6	<0.3 ^f		6, 7/2 ⁺
9/2 ⁻	611.2	114.4	2.1(2)	0.88(7)	3, 5/2 ⁻
		378.1	52(4)	0.75(1)	6, 7/2 ⁺
		356.4	4.2(5)	0.69(3)	9, 7/2 ⁺
		305.7	2.6(6)	0.81(5)	1, 11/2 ⁻
		83.7	1.0(3)		Misc
13/2 ⁻	853.1	241.9	52(4)	0.85(1)	3, 9/2 ⁻
17/2 ⁻	1216.7	363.6	58(5)	0.92(1)	3, 13/2 ⁻
21/2 ⁻	1678.9	462.2	57(5)	0.98(2)	3, 17/2 ⁻
25/2 ⁻	2214.0	535.1	50(5)	1.07(2)	3, 21/2 ⁻
29/2 ⁻	2810.2	596.2	27(2)	0.93(2)	3, 25/2 ⁻
33/2 ⁻	3392.7	582.5	26(6)	1.04(1) ^g	3, 29/2 ⁻
37/2 ⁻	3974.3	581.6	21(6)	1.04(1) ^g	3, 33/2 ⁻
41/2 ⁻	4557.3	583.0	17(4)	1.04(1) ^g	3, 37/2 ⁻
45/2 ⁻	5186.7	629.4	13(1)	1.11(2)	3, 41/2 ⁻
49/2 ⁻	5890.3	703.6	6.5(8)	1.01(3)	3, 45/2 ⁻
		683.7	0.9(4)		4, 45/2 ⁻
53.2 ⁻	6643.0	752.7	5.3(5)	1.04(3)	3, 49/2 ⁻
57/2 ⁻	7438.7	795.7	2.8(4)	0.98(3)	3, 53/2 ⁻
		764.4	<0.3		5, 53/2 ⁻
61/2 ⁻	8294.3	855.6	1.9(3)	1.13(5)	3, 57/2 ⁻
65/2 ⁻	9206.9	912.6	0.8(4)		3, 61/2 ⁻
69/2 ⁻	10 158.8	951.9	<0.3		3, 65/2 ⁻
Band 4: $\alpha = +1/2$					
45/2 ⁻	5206.7	649.4	2.2(3)	0.94(4)	3, 41/2 ⁻
(49/2 ⁻)	5849.6	642.9	0.4(1)		4, 45/2 ⁻
		334.8	0.5(1)		4, 47/2 ⁻
		662.9	1.3(2)		3, 45/2 ⁻
(53/2 ⁻)	6593.3	743.7	0.8(1)		4, (49/2 ⁻)
(57/2 ⁻)	7405.5	812.2	0.6(1)		4, (53/2 ⁻)
(61/2 ⁻)	8278.1	872.6	<0.3		4, (57/2 ⁻)

TABLE I. (Continued.)

I^π ^a	E_{level} (keV)	E_γ (keV) ^b	I_γ ^c	R_{ang}	Band _{f} , I_f ^d
(65/2 ⁻)	9204.8	926.7	<0.3		4, (61/2 ⁻)
Band 4: $\alpha = -1/2$					
(47/2 ⁻)	5514.8	308.1	0.8(1)		4, 45/2 ⁻
		328.0	0.6(1)		3, 45/2 ⁻
(51/2 ⁻)	6205.8	740.7	1.7(2)		1, (47/2 ⁻)
(55/2 ⁻)	6987.7	781.9	1.5(2)		4, (51/2 ⁻)
(59/2 ⁻)	7830.3	842.6	1.3(2)		4, (55/2 ⁻)
(63/2 ⁻)	8744.9	914.6	0.9(1)		4, (59/2 ⁻)
Band 5					
53/2 ⁻	6674.3	784.0	1.5(2)	0.84(5)	3, 49/2 ⁻
57/2 ⁻	7471.7	797.4	0.9(2)		5, 53/2 ⁻
		828.8	1.2(1)		3, 53/2 ⁻
61/2 ⁻	8324.4	852.7	1.4(2)		5, 57/2 ⁻
65/2 ⁻	9222.6	898.2	0.8(1)		5, 61/2 ⁻
69/2 ⁻	10 143.7	921.1	0.3(1)		5, 65/2 ⁻
Band 6: $\pi d_{3/2}[411]1/2 \alpha = -1/2$					
3/2 ⁺	0.0				
7/2 ⁺	233.1	233.1	56(6) ^e	0.83(2)	6, 3/2 ⁺
		138.1	6.0(6) ^e	0.69(4)	7, 5/2 ⁺
11/2 ⁺	610.6	377.5	22(2)	0.84(2)	6, 7/2 ⁺
15/2 ⁺	1091.2	480.6	19(2)	0.95(5)	6, 11/2 ⁺
19/2 ⁺	1638.9	547.7	15(2)	1.02(3)	6, 15/2 ⁺
23/2 ⁺	2222.2	583.3	9.6(9)	1.09(3)	6, 19/2 ⁺
27/2 ⁺	2821.2	599.0	2.9(5)	0.78(4)	6, 23/2 ⁺
31/2 ⁺	3346.4	525.2	0.9(4)		6, 27/3 ⁺
35/2 ⁺	3880.8	534.4	0.3(2)		6, 31/2 ⁺
39/2 ⁺	4489.5	608.7	<0.3		6, 35/2 ⁺
Band 6: $\pi d_{3/2}[411]1/2 \alpha = +1/2$					
5/2 ⁺	175.9	175.9	~ 4 ^e	0.72(7)	6, 3/2 ⁺
9/2 ⁺	503.2	327.3	8(2)	0.85(5)	6, 5/2 ⁺
		270.2	8(2)	0.81(5)	6, 7/2 ⁺
13/2 ⁺	940.1	436.9	12(2)	0.97(6)	6, 9/2 ⁺
		329.5	2.9(7)		6, 11/2 ⁺
17/2 ⁺	1456.9	516.8	8(3)		6, 13/2 ⁺
		365.7	2.1(6)	0.62(4)	6, 15/2 ⁺
21/2 ⁺	2019.4	562.5	4.8(8)		6, 17/2 ⁺
		380.5	0.9(4)		6, 19/2 ⁺
Band 7: $\pi d_{3/2}[402]5/2 \alpha = +1/2$					
5/2 ⁺	94.9	94.9	~ 64 ^e	0.73(5)	6, 3/2 ⁺
9/2 ⁺	375.0	280.1	26(2)	0.83(4) ^g	7, 5/2 ⁺
		169.6	69(4)	0.81(2)	7, 7/2 ⁺
		120.0	28(1)	0.84(6)	9, 7/2 ⁺
13/2 ⁺	791.2	416.2	83(6)	0.91(2)	7, 9/2 ⁺
		216.3	55(4)	0.79(1) ^g	7, 11/2 ⁺
		134.1	5.4(4)	0.81(8)	9, 11/2 ⁺
17/2 ⁺	1285.3	494.1	95(7)	0.93(2)	7, 13/2 ⁺
		248.9	49(4)	0.79(2)	7, 15/2 ⁺
		128.9	2.7(2)		9, 15/2 ⁺
21/2 ⁺	1820.2	534.9	$\equiv 100$	0.95(4)	7, 17/2 ⁺
		262.7	39(4)	0.79(4)	7, 19/2 ⁺
25/2 ⁺	2328.0	507.8	77(6)	1.01(5) ^g	7, 21/2 ⁺
		239.0	55(5)	0.77(2) ^g	7, 23/2 ⁺
29/2 ⁺	2781.0	453.0	36(3)	0.97(3)	7, 25/2 ⁺
		214.7	61(5)	0.79(1) ^g	7, 27/2 ⁺

TABLE I. (*Continued.*)

I^π ^a	E_{level} (keV)	E_γ (keV) ^b	I_γ ^c	R_{ang}	Band _{f} , I_f ^d
33/2 ⁺	3212.0	431.0	22(2)	0.91(4)	7, 29/2 ⁺
		243.7	36(3)	0.75(12)	7, 31/2 ⁺
		204.5	7.1(7)	0.66(4)	8, 31/2 ⁺
37/2 ⁺	3720.8	396.6	3.8(6)	0.78(4)	Misc, 29/2 ⁺
		508.8	29(4)	1.01(5) ^g	7, 33/2 ⁺
		294.0	24(2)	0.72(4)	7, 35/2 ⁺
41/2 ⁺	4304.7	246.7	5.9(6)		8, 35/2 ⁺
		583.9	31(3)	1.14(4)	7, 37/2 ⁺
		313.8	22(4)	0.74(2) ^g	7, 39/2 ⁺
45/2 ⁺	4920.5	278.8	5.4(7)	0.83(4) ^g	8, 39/2 ⁺
		615.8	23(4)	1.07(3) ^g	7, 41/2 ⁺
		312.5	20(4)	0.74(2) ^g	7, 43/2 ⁺
49/2 ⁺	5550.4	629.9	20(2)	1.03(14)	7, 45/2 ⁺
		314.4	13(3)	0.74(2) ^g	7, 47/2 ⁺
53/2 ⁺	6221.7	671.3	17(2)	0.98(6)	7, 49/2 ⁺
		333.4	11(2)	0.73(3)	7, 51/2 ⁺
57/2 ⁺	6963.5	741.8	15(2)	1.06(6)	7, 53/2 ⁺
		364.7	13(2)	0.68(5)	7, 55/2 ⁺
61/2 ⁺	7785.9	822.4	14(2)	0.88(6)	7, 57/2 ⁺
		396.7	7.1(7)	0.77(4)	7, 59/2 ⁺
65/2 ⁺	8685.5	899.6	8.4(8)	0.97(7)	7, 61/2 ⁺
		421.9	2.7(4)		7, 63/2 ⁺
69/2 ⁺	9654.2	968.7	4.8(5)		7, 65/2 ⁺
73/2 ⁺	10 681.4	1027.2	2.3(4)		7, 69/2 ⁺
77/2 ⁺	11 756.6	1075.2	1.2(2)		7, 73/2 ⁺
81/2 ⁺	12 872.0	1115.4	0.4(2)		7, 77/2 ⁺
85/2 ⁺	14 025.7	1153.7	<0.3		7, 81/2 ⁺
Band 7: $\pi d_{5/2}[402]5/2 \alpha = -1/2$					
7/2 ⁺	205.5	110.6	$\sim 47^e$	0.74(4)	7, 5/2 ⁺
11/2 ⁺	574.9	369.4	63(4)	0.84(3)	7, 7/2 ⁺
		199.9	62(5)	0.82(2)	7, 9/2 ⁺
		143.1	4.1(4)	0.86(9)	9, 9/2 ⁺
		319.8	6.6(8)		9, 7/2 ⁺
15/2 ⁺	1036.5	461.6	93(7)	0.90(3)	7, 11/2 ⁺
		245.2	50(5)	0.72(3)	7, 13/2 ⁺
		97.0	<0.3		6, 13/2 ⁺
19/2 ⁺	1557.5	521.0	93(7)	1.33(3)	7, 15/2 ⁺
		272.4	38(4)	0.81(6)	7, 17/2 ⁺
23/2 ⁺	2089.1	531.6	90(7)	1.09(7)	7, 19/2 ⁺
		268.8	42(4)	0.66(5)	7, 21/2 ⁺
27/2 ⁺	2566.4	477.3	49(4)	1.22(7)	7, 23/2 ⁺
		238.3	65(5)	0.77(2)	7, 25/2 ⁺
31/2 ⁺	2968.3	401.9	15(2)	0.87(4)	7, 27/2 ⁺
		187.2	32(2)	0.71(2)	7, 29/2 ⁺
		153.2	2.5(2)	0.62(10)	Misc, 29/2 ⁺
		333.3	5.8(5)	0.90(5)	Misc, 27/2 ⁺
35/2 ⁺	3426.9	458.6	30(3)	1.09(8)	7, 31/2 ⁺
		214.9	30(4)	0.79(1) ^g	7, 33/2 ⁺
39/2 ⁺	3991.0	564.1	38(3)	1.19(5)	7, 35/2 ⁺
		270.1	23(2)	0.68(3)	7, 37/2 ⁺
43/2 ⁺	4608.0	617.0	25(3)	1.07(3) ^g	7, 39/2 ⁺
		303.3	23(2)	0.74(2)	7, 41/2 ⁺
		247.6	1.9(4)		8, 41/2 ⁺
		582.0	9.4(9)	0.80(8)	8, 39/2 ⁺
47/2 ⁺	5235.9	627.9	23(2)	1.04(9)	7, 43/2 ⁺
		315.5	22(4)	0.74(2) ^g	7, 45/2 ⁺

TABLE I. (Continued.)

I^π ^a	E_{level} (keV)	E_γ (keV) ^b	I_γ ^c	R_{ang}	Band _{f} , I_f ^d
51/2 ⁺	5888.3	652.4	20(2)	1.10(8)	7, 47/2 ⁺
		338.0	14(1)	0.75(3)	7, 49/2 ⁺
55/2 ⁺	6598.8	710.5	13(1)	1.16(5)	7, 51/2 ⁺
		377.2	13(1)	0.69(3)	7, 53/2 ⁺
59/2 ⁺	7389.1	790.3	12(1)	0.92(6)	7, 55/2 ⁺
		425.7	10(1)		7, 57/2 ⁺
63/2 ⁺	8263.4	874.3	10(1)	0.96(12)	7, 59/2 ⁺
		477.7	5.8(8)		7, 61/2 ⁺
67/2 ⁺	9219.5	956.1	6.0(7)	0.96(7)	7, 63/2 ⁺
71/2 ⁺	10 250.3	1030.8	1.8(4)		7, 67/2 ⁺
75/2 ⁺	11 346.0	1095.7	0.8(4)		7, 71/2 ⁺
79/2 ⁺	12 486.1	1140.1	0.3(2)		7, 75/2 ⁺
Band 8: $\pi h_{11/2} AF \alpha = +1/2$					
33/2 ⁺	3253.3	245.7	24(3)	0.74(5)	8, 31/2 ⁺
37/2 ⁺	3772.5	519.2	16(2)	1.12(9)	8, 33/2 ⁺
		298.2	13(2)	0.80(4)	8, 35/2 ⁺
41/2 ⁺	4360.7	588.2	11(1)	1.09(15)	8, 37/3 ⁺
		334.2	5.0(5)	0.78(8)	8, 39/2 ⁺
45/2 ⁺	5009.1	648.4	6.7(7)	0.80(6)	8, 41/2 ⁺
		350.4	6.0(6)	0.94(14)	8, 43/2 ⁺
49/2 ⁺	5697.8	688.7	6.1(6)	1.03(11) ^g	8, 45/2 ⁺
		352.4	1.0(1)		8, 47/2 ⁺
53/2 ⁺	6422.2	724.4	4.8(5)		8, 49/2 ⁺
		367.2	3.3(4)		8, 51/2 ⁺
57/2 ⁺	7214.3	792.1	2.5(3)		8, 53/2 ⁺
		397.9	1.7(2)		8, 55/2 ⁺
61/2 ⁺	8085.8	871.5	2.1(2)		8, 57/2 ⁺
65/2 ⁺	9030.9	945.1	1.5(2)		8, 61/2 ⁺
69/2 ⁺	10 020.3	989.4	0.8(1)		8, 65/2 ⁺
(73/2 ⁺)	(11 032)	(1012)	<0.3		8, 69/2 ⁺
Band 8: $\pi h_{11/2} AF \alpha = -1/2$					
31/2 ⁺	3007.6	441.3	20(2)	1.00(5)	7, 27/2 ⁺
		226.6	32(3)	0.72(2)	7, 29/2 ⁺
35/2 ⁺	3474.3	466.7	28(3)	0.99(4)	8, 31/2 ⁺
		221.1	8.3(9)	0.59(8)	8, 33/2 ⁺
		262.2	8.8(9)	0.64(4)	7, 33/2 ⁺
39/2 ⁺	4026.3	552.0	19(2)	0.99(6)	8, 35/2 ⁺
		253.9	8.6(8)		8, 37/2 ⁺
43/2 ⁺	4658.6	632.3	6.9(7)	0.97(10)	8, 39/2 ⁺
		298.0	4.6(5)	0.80(4)	8, 41/2 ⁺
		667.3	14(2)	1.00(7)	7, 39/2 ⁺
47/2 ⁺	5345.4	686.8	11(1)	1.03(11) ^g	8, 43/2 ⁺
		336.4	4.4(5)		8, 45/2 ⁺
51/2 ⁺	6054.8	709.4	6.9(7)	1.13(13)	8, 47/2 ⁺
		357.1	1.7(2)		8, 49/2 ⁺
55/2 ⁺	6816.2	761.4	3.8(4)		8, 51/2 ⁺
		394.2	0.9(1)		8, 53/2 ⁺
59/2 ⁺	7654.7	838.5	2.7(3)		8, 55/2 ⁺
63/2 ⁺	8564.6	909.9	1.2(1)		8, 59/2 ⁺
Band 9: $\pi g_{7/2}[404]7/2 \alpha = +1/2$					
9/2 ⁺	432.2	337.1	$\sim 11^e$	0.99(8)	7, 5/2 ⁺
		177.3	$\sim 21^f$	0.75(4)	9, 7/2 ⁺
13/2 ⁺	874.5	442.3	11(1)	0.87(4)	9, 9/2 ⁺
		217.5	4.0(5)	0.92(8)	9, 11/2 ⁺
17/2 ⁺	1394.5	520.0	9(1)	0.87(4)	9, 13/2 ⁺

TABLE I. (*Continued.*)

I^π ^a	E_{level} (keV)	E_γ (keV) ^b	I_γ ^c	R_{ang}	Band _{f} , I_f ^d
21/2 ⁺	1950.7	556.2	5.8(7)	1.12(7)	9, 17/2 ⁺
25/2 ⁺	2463.1	512.4	3.5(5)		9, 21/2 ⁺
		642.7	5.4(6)		7, 21/2 ⁺
Band 9: $\pi g_{7/2}[404]7/2 \alpha = -1/2$					
7/2 ⁺	254.9	160.0	$\sim 68^\circ$	0.76(3)	7, 5/2 ⁺
11/2 ⁺	656.9	402.0	11(2)		9, 7/2 ⁺
		224.8	7.5(9)	0.86(20)	9, 9/2 ⁺
15/2 ⁺	1156.5	499.6	7.9(9)		9, 11/2 ⁺
		282.2	1.4(3)		9, 13/2 ⁺
19/2 ⁺	1722.9	566.4	3.3(4)		9, 15/2 ⁺
Band 10: $\pi i_{13/2}[660]1/2$					
21/2 ⁺	2057.2	771.9	1.7(2)	1.06(8)	7, 17/2 ⁺
		600.3	1.9(3)		6, 17/2 ⁺
25/2 ⁺	2477.7	420.5	3.5(4)	0.96(3)	10, 21/2 ⁺
		526.9	4.2(5)	0.96(3)	9, 21/2 ⁺
		458.1	1.0(2)		6, 21/2 ⁺
29/2 ⁺	2963.1	485.4	8.3(8)	0.96(2)	10, 25/2 ⁺
		500.0	3.3(3)	1.04(4)	9, 25/2 ⁺
33/2 ⁺	3480.5	517.4	12(1)	0.95(2)	10, 29/2 ⁺
37/2 ⁺	4045.5	565.0	11(1)	0.93(2)	10, 33/2 ⁺
41/2 ⁺	4661.3	615.8	10(1)	1.09(2)	10, 37/2 ⁺
45/2 ⁺	5326.5	665.2	9.0(9)	1.08(2)	10, 41/2 ⁺
49/2 ⁺	6035.9	709.4	6.9(7)	1.19(4)	10, 45/2 ⁺
53/2 ⁺	6780.2	744.3	6.1(6)	1.02(3)	10, 49/2 ⁺
57/2 ⁺	7566.1	785.9	4.0(2)	0.96(6)	10, 53/2 ⁺
61/2 ⁺	8398.9	832.8	2.3(2)	0.91(3)	10, 57/2 ⁺
65/2 ⁺	9280.3	881.4	1.7(2)	0.99(5)	10, 61/2 ⁺
69/2 ⁺	10 214.1	933.8	1.0(2)		10, 65/2 ⁺
73/2 ⁺	11 200.7	986.6	0.8(4)		10, 69/2 ⁺
77/2 ⁺	12 240.7	1040.0	0.3(2)		10, 73/2 ⁺
(81/2 ⁺)	(13 343)	(1103)	<0.3		10, 77/2 ⁺
Band 11: $n_w = 1$					
35/2 ⁺	4133.5	653.0	0.4(1)		10, 33/2 ⁺
39/2 ⁺	4688.1	554.6	0.3(1)		11, 35/2 ⁺
		642.6	0.6(1)	0.50(8)	10, 37/2 ⁺
43/2 ⁺	5293.8	605.7	0.8(1)		11, 39/2 ⁺
		632.3	0.8(1)	0.71(8)	10, 41/2 ⁺
47/2 ⁺	5949.9	656.1	1.2(2)		11, 43/2 ⁺
		623.2	0.8(1)		10, 45/2 ⁺
51/2 ⁺	6654.2	704.3	1.1(2)		11, 47/2 ⁺
		(618)	<0.3		10, 49/2 ⁺
55/2 ⁺	7406.6	752.4	0.9(2)		11, 51/2 ⁺
59/2 ⁺	8206.1	799.5	0.8(1)		11, 55/2 ⁺
63/2 ⁺	9054.8	848.7	0.7(1)		11, 59/2 ⁺
67/2 ⁺	9954.6	899.8	0.5(1)		11, 63/2 ⁺
71/2 ⁺	10 906.6	952.0	0.3(1)		11, 67/2 ⁺
75/2 ⁺	11 911.3	1004.7	<0.3		11, 71/2 ⁺
79/2 ⁺	12 968.4	1057.1	<0.3		11, 75/2 ⁺
Band 12					
53/2 ⁺	6800.2	764.3	1.1(1)	1.03(6)	10, 49/2 ⁺
57/2 ⁺	7596.6	796.4	0.8(1)	1.05(6)	12, 53/2 ⁺
		(816)	<0.3		10, 53/2 ⁺
61/2 ⁺	8437.5	840.9	0.7(1)		12, 57/2 ⁺
65/2 ⁺	9332.1	894.6	0.4(1)		12, 61/2 ⁺

TABLE I. (Continued.)

I^π ^a	E_{level} (keV)	E_γ (keV) ^b	I_γ ^c	R_{ang}	Band _f , I_f ^d
69/2 ⁺	10 267.6	935.5	<0.3		12, 65/2 ⁺
(73/2 ⁺)	(11 240)	(972)	<0.3		12, 69/2 ⁺
Miscellaneous levels					
	527.8	321.4	~9 ^e		1, 9/2 ⁻
	2234.4	592.8	3.2(3)		2a, 17/2 ⁻
27/2 ⁺	2635.0	546.0	16(2)		7, 23/2 ⁺
29/2 ⁺	2815.1	487.1	13(1)		7, 25/2 ⁺
		248.7	4.7(5)		7, 27/2 ⁺
		180.3	3.8(4)		Misc., 27/2 ⁺

^aSpin and parity of the depopulated state.

^bUncertainties in γ -ray energies are 0.2 keV for most transitions, except for relatively weak transitions (<1) where 0.5-keV uncertainties are appropriate.

^cRelative intensity of the transition with respect to the intensity of the 534.9-keV transition in band 7.

^dIndicates the band and the state to which the γ ray decays. The notation Misc. refers to the miscellaneous levels recorded at the end of this table.

^eEstimated based on total intensity balance.

^fEstimated based on total intensity balance and branching ratio.

^gUnresolved doublet.

obtained. A ratio $R_{\text{ang}} = W(\theta_b)/W(\theta_{90^\circ})$ could be calculated and normalized such that known $E1$ and $E2$ transitions have values of approximately 0.6 and 1.0, respectively. Because no conclusive spin assignments were made in the decay studies into ^{167}Ta [12], all of the absolute spin assignments must be regarded as tentative in the level schemes proposed in Figs. 1 and 2. However, the relative spins of the levels and bands are firm. Only tentative levels and transitions in bands where no relative spin assignment could be obtained based on linking transitions are designated in parentheses. The energies and proposed spins of the observed states in ^{167}Ta , as well as the energies, intensities, and R_{ang} ratios of the γ -ray transitions, are provided in Table I.

III. LEVEL SCHEME

Only two published works [12,13] describing excited states of ^{167}Ta were available previous to this work. Both of these tentatively assigned $3/2^+$ quantum numbers to the ground state; this assignment is consistent with the lowest level observed in the present experiment. Meissner *et al.* [12] observed γ -ray transitions following the decay of ^{167}W and reported 11 excited states and 16 transitions. Seven of those states and eight of the γ rays could be confirmed in the present experiment. Theine *et al.* [13] observed four rotational bands in the $p4n$ side channel of the $^{30}\text{Si} + ^{142}\text{Nd}$ reaction. This group used the ESSA30 array that consisted of 29 Compton-suppressed Ge spectrometers. In this work, the bands labeled 1, 2, 3, and 7 in Figs. 1 and 2 were observed up to spins $35/2$, $59/2$, $41/2$, and $45/2$, respectively. A total of 111 transitions were assigned to ^{167}Ta in Ref. [13] and are confirmed here, although several γ rays have been placed differently in the level scheme.

The present level scheme contains 12 rotational structures and more than 370 transitions assigned to ^{167}Ta . The bands associated with negative parity are found in Fig. 1, while

those associated with positive parity are displayed in Fig. 2. Transitions linking band 3 to bands 6 and 9 (see Fig. 1) allow for the excitation energies of all the bands to be established for the first time.

A. Band 1

Band 1 in Fig. 1 was previously identified and its band-head state was assigned $9/2^-$ in Ref. [13], based upon systematics of similar bands in heavier tantalum nuclei and $N = 94$ isotones. However, the energy of the bandhead had not been determined in the earlier works. Owing to the various linking transitions between bands 1, 2, 3, and 4 shown in Fig. 1, the excitation energy is now firmly established at 206.4 keV. This is an example where the study of high-spin states can reveal important information regarding the excitation of particle/hole states at low spins and energies. The angular-correlation ratios for the linking transitions between bands 1 and 2, bands 2 and 3, as well as bands 3 and 6 (see Table I) confirm the spin-parity assignment displayed in Fig. 1, assuming that the lowest state observed ($3/2^+$ in band 6) is indeed the ground state. Band 1 was extended from $35/2^-$ up to $83/2^-$ and a summed coincidence spectrum displaying the transitions associated with this sequence is given in Fig. 3(a). The states below $I = 29/2^-$ are very strongly fed, which is consistent with the fact that band 1 is the yrast sequence below this spin. Figure 4 plots the excitation energies of the states (minus a rotor reference) versus spin such that the yrast states can be discerned.

B. Bands 2 and 2a

The sequence labeled band 2 in Fig. 1 was previously observed from $29/2^-$ to $59/2^-$ with three linking transitions (157, 404, and 657 keV) feeding into band 1 [13]. Relative spin assignments for band 2 could be confirmed from the angular-correlation ratios of the 404-, 540-, and 657-keV

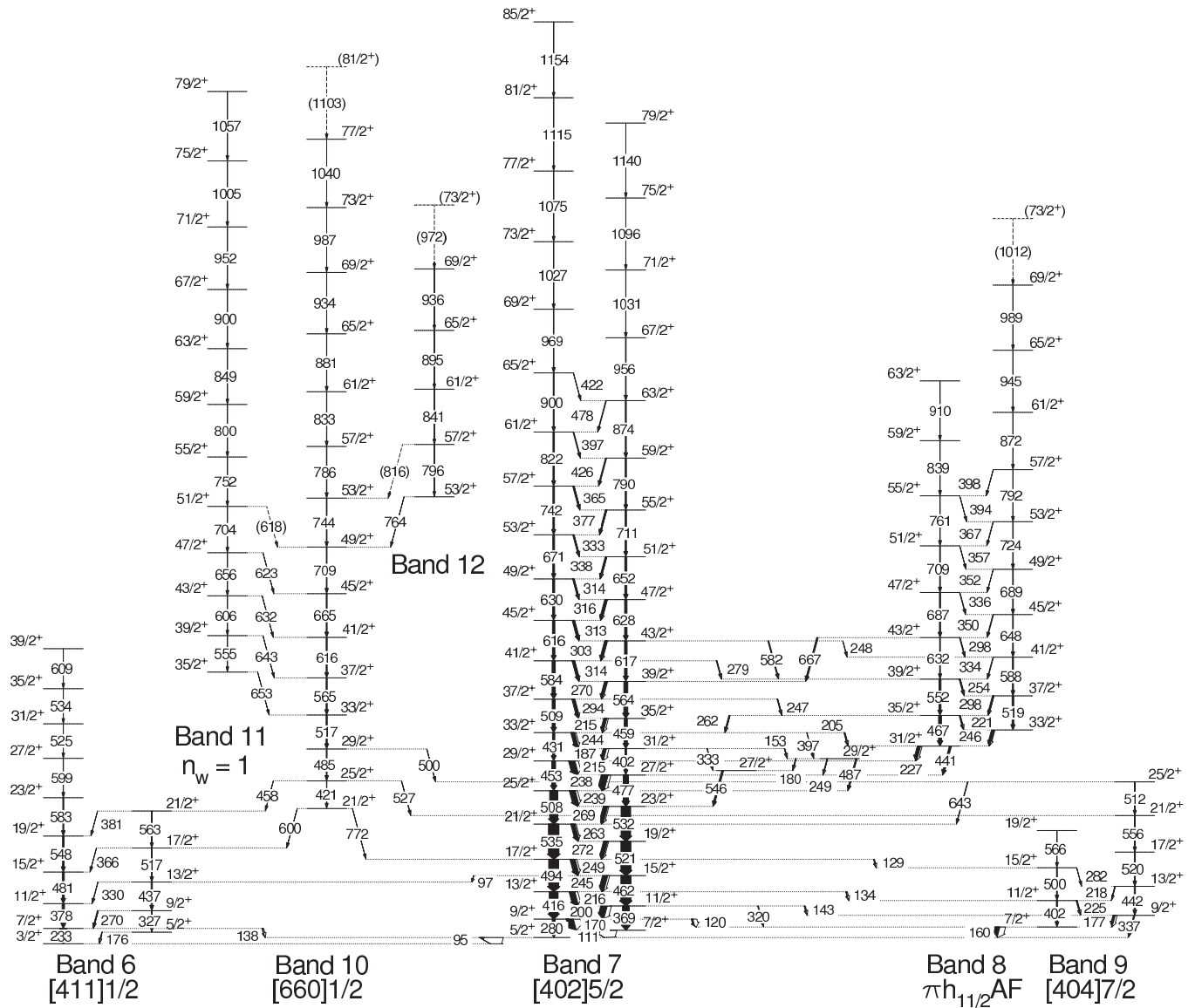


FIG. 2. Partial level scheme for ^{167}Ta displaying the positive-parity structures. Tentative transitions and levels are denoted with dashed lines.

regarded as tentative. Further confirmation of the presence of a triplet comes from the interactions of band 4 with bands 1 and 3 (see Sec. III D). If a doublet was assumed, the correct interactions could not have been delineated. The spectrum displayed in Fig. 5(a) identifies the transitions that allowed this sequence to be extended to $69/2^-$ and it displays some of the transitions of band 5.

D. Bands 4 and 5

Two bands observed at higher spins were newly identified and are displayed in Fig. 1 as bands 4 and 5. The lowest observed level in band 4 decays to band 3 through the 649-keV transition with $R_{\text{ang}} = 0.94(4)$, indicating that the transition is of $E2$ character. This assignment implies that the $45/2^-$ states in bands 3 and 4 are nearly degenerate (differing by only 20 keV) which would then explain the 663- and 684-

keV linking transitions from the $49/2^-$ levels of both bands. A probable $47/2^-$ level is found assuming that the 308- and 335-keV lines are dipole in nature. In addition, a sequence of transitions is found above a possible $51/2^-$ level, which is nearly degenerate (~ 24 keV) with the $51/2^-$ state in band 1. Surprisingly, the possible $E2$ transition connecting the $51/2^-$ and $47/2^-$ states is missing in band 4, which may mean that the two structures are unrelated. However, when the energies of these sequences are plotted in Fig. 4(a), one observes that they are likely partner bands; thus, it is assumed these two sequences are parts of the same intrinsic structure.

A short sequence of transitions (band 5) was found to feed into band 3 at $I = 49/2^-$ and $53/2^-$, as discussed above. The $R_{\text{ang}} = 0.84(5)$ value of the 784-keV line and the observation of the cross transitions from the $57/2^-$ states from both bands 3 and 5 strongly imply that these states are mixed such that they have the same spin and parity. As can be seen in Fig. 4(a), band

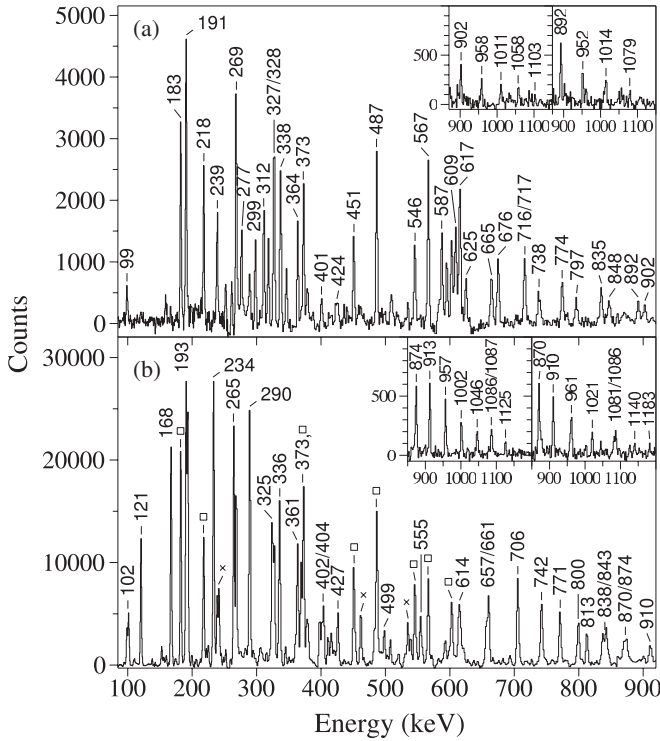


FIG. 3. (a) Spectra for band 1 in ^{167}Ta . The main spectrum was produced by summing the triple gates of the 631-keV transition with any two $E2$ transitions in the $\alpha = -1/2$ signature above the $31/2^-$ state along with triple coincidence gates of the 621-keV line with any two $E2$ transitions in the $\alpha = +1/2$ signature above the $29/2^-$ state. The left inset is the result of summing all possible triple combinations using $E2$ transitions in the $\alpha = -1/2$ signature above the $31/2^-$ state. In a similar manner, the right inset is the spectrum from summing all possible triple combinations using $E2$ transitions in the $\alpha = +1/2$ signature above the $29/2^-$ level. (b) Spectra for band 2. All possible triple combinations of the $M1$ transitions from the $29/2^-$ level to the $43/2^-$ state produced the main spectrum. All possible triple combinations of the $E2$ transitions in the $\alpha = -1/2$ sequence above the $43/2^-$ state were summed for the left inset. The right inset is a summed spectrum of all possible triple combinations of $E2$ transitions in the $\alpha = +1/2$ signature above the $41/2^-$ level. Squares indicate transitions from band 1, while crosses denote γ rays from band 3.

5 is nearly degenerate with band 3 and it appears to become lower in energy than the latter band at the highest spin.

E. Band 6

Only the 233-keV transition was previously identified in Refs. [12,13], which feeds directly the presumed $3/2^+$ ground state. This is likely attributable to the fact that the next $E2$ transition has the same energy (378 keV) as the linking transition from band 3; thus, the $11/2^+$ and $9/2^-$ states from bands 6 and 3, respectively, are within 1 keV of each other. With the use of triple coincidence gates, this weakly coupled band could be established as seen in Fig. 2 and a spectrum is provided in Fig. 5(b). The energetically favored $\alpha = -1/2$ sequence was extended to $39/2^+$, while the

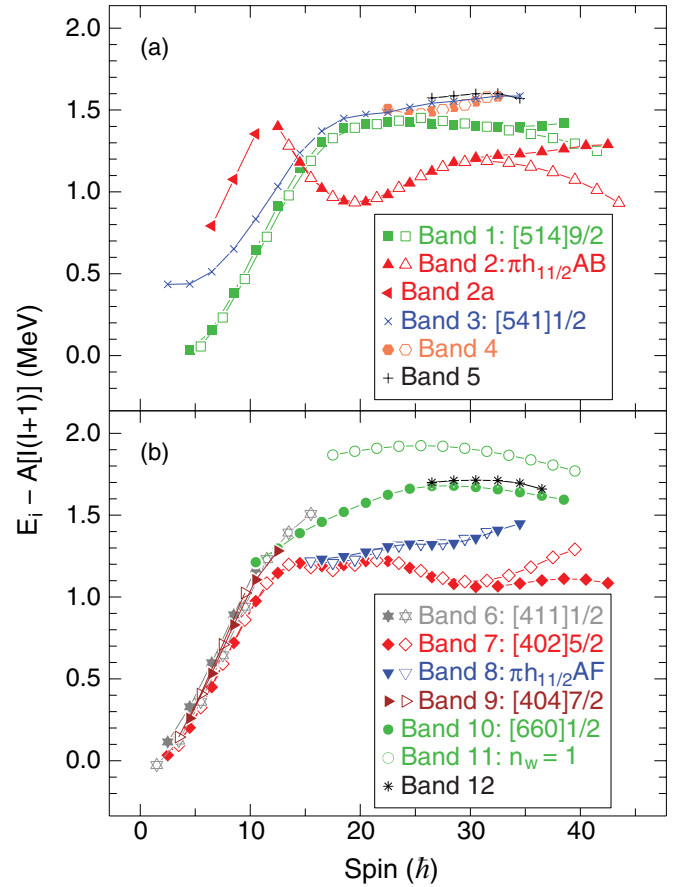


FIG. 4. (Color online) Excitation energies of the observed levels minus a rigid-rotor reference, where this reference was assumed to have a moment of inertia parameter $A = 0.007$ MeV. The odd-parity bands 1–5 are displayed in panel (a), while the even-parity bands 6–12 are in panel (b). Positive (negative) signatures are represented with solid (open) symbols.

unfavored $\alpha = +1/2$ sequence was only delineated to $21/2^+$ and is fed by band 10 (see Sec. III I). Although band 6 is close in energy to band 7 (one of the more strongly fed bands in ^{167}Ta), as seen in Fig. 4(b), the former is significantly less intense. The high-spin portion of band 6 appears to move away from the yrast line above $I = 29/2^+$, where the reaction predominantly feeds the discrete states [see Fig. 4(b)]. This may explain why band 6 could not be observed to higher spin and is one of the weaker bands in ^{167}Ta .

F. Band 7

The structure labeled Band 7 in Fig. 2 was previously observed up to a spin of $45/2^+$ [13]. The 95-keV γ ray linking the lowest state in band 7 to the $3/2^+$ ground state and the 138-keV line from the $7/2^+$ level in band 6 to this same state could both be assigned as dipole transitions (see Table I), thus confirming the $I = 5/2$ assignment. Positive parity is assumed, based upon the configuration assignment (see Sec. III F). Figure 6(a) displays spectra that were used to extend the band up to $85/2^+$. With the increased statistics and ability to place triple coincidence gates in the hypercube

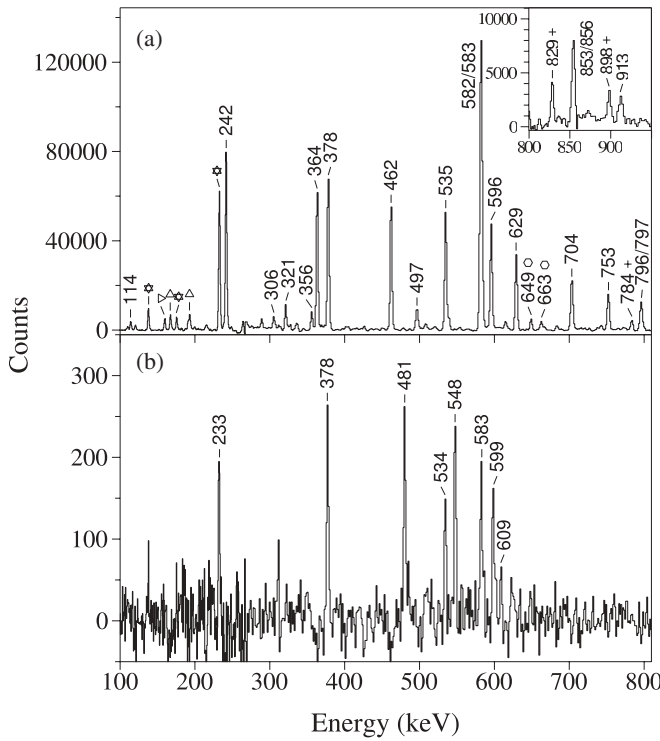


FIG. 5. (a) Spectrum of band 3 resulting from a sum of gates on all $E2$ transitions in the structure. The inset is a continuation of the main spectrum. Peaks marked with triangles, hexagons, plus signs, stars, and right-pointing triangles are from bands 2, 4, 5, 6, and 9, respectively. (b) Spectrum of band 6 produced by summing all clean triple gates using the 525-keV transition with other $E2$ transitions in the $\alpha = -1/2$ sequence.

the ordering of transitions near $45/2^+$ was slightly modified from that given in Ref. [13]. Several low-energy transitions were found deexciting the band toward band 9 at lower spins, while many interband transitions were also observed between bands 7 and 8. These latter two bands lie close in energy in the $I = 31/2$ to $43/2$ spin range, as can be seen in Fig. 4(b), an observation that accounts for the numerous linking transitions. There are also two states (with $I = 27/2$ and $29/2$) not directly associated with either bands 7 or 8, but fed by γ rays originating from these structures. Band 7 defines the yrast sequence of ^{167}Ta in the range of $I = 55/2$ to $73/2\hbar$ [Fig. 4(b)].

G. Band 8

A new, higher-lying, strongly coupled sequence was observed in the present experiment and is labeled as band 8 in Fig. 2. The 441- and 667-keV transitions deexciting the $31/2^+$ and $43/2^+$ states, respectively, were determined to both have $R_{\text{ang}} \approx 1$. Thus, they may be classified as stretched- $E2$ transitions herewith fixing the spin of band 8 as proposed in Fig. 2 and with the same positive parity as band 7. A spectrum of band 8 can be found in Fig. 6(b), where one may observe the strong coincidence with band 7 whose transitions are denoted with open diamonds. The structure could be extended up to $I = 73/2^+$.

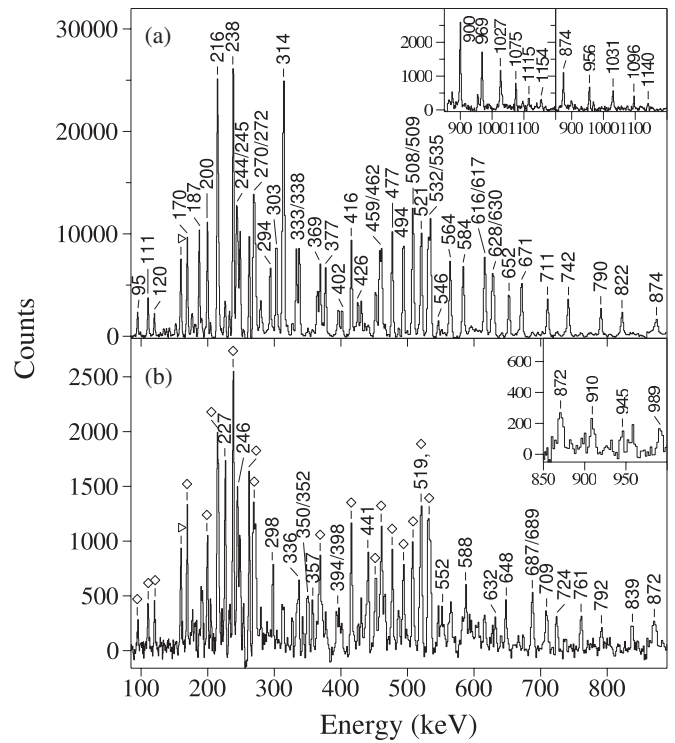


FIG. 6. (a) Spectrum of band 7 resulting from a sum of triple-gated coincidence spectra using all combinations of $M1$ transitions from the $31/2^+$ level to the $45/2^+$ state. The left inset is a spectrum generated by summing all combinations of the $E2$ transitions in the $\alpha = +1/2$ sequence above the $45/2^+$ state. The right inset was constructed in a similar way with all combinations of triple gates with $E2$ transitions above the $47/2^+$ state in the $\alpha = -1/2$ signature. (b) Spectrum of band 8 resulting from a sum of as many clean triple gates from intraband transitions as possible. The inset is simply a continuation of the main spectrum. Peaks denoted with diamonds and right-pointing triangles are associated with bands 7 and 9, respectively.

H. Band 9

A short sequence, labeled as band 9 in Fig. 2, was identified which is primarily fed by bands 7 and 10. The band-head state was first observed in Ref. [12], and evidence of this level was also seen in Ref. [13]. However, the latter reversed the ordering of the 120- and 160-keV transitions. The observation of the 320-keV line from the $11/2^+$ level in band 7 to the $7/2^+$ state in band 9 confirms the placement of the level at 255 keV, in agreement with Ref. [12]. The angular-correlation ratios of the 160- and 337-keV lines of 0.76(3) and 0.99(8), respectively, allow for the assignment of spins as shown in Fig. 2 and indicates that positive parity is associated with band 9.

I. Bands 10, 11, and 12

The new, decoupled sequences labeled bands 10, 11, and 12 in Fig. 2 were previously discussed in Ref. [4]; spectra for these bands may be found in that publication. Band 10 feeds bands 6, 7, and 9 where the angular-correlation ratios for the 772-, 527-, and 500-keV γ rays were all found to be

consistent with values for stretched $E2$ transitions (see Table I). This allowed for confident spin and parity assignments for the structure. Angular-correlation ratios of 0.50(8) and 0.71(8) were determined for the 643- and 632-keV lines from band 11 to band 10, indicating that they are $\Delta I = 1$ in nature. Thus, the spins of band 11 could be deduced and the parity is assumed to be positive based on the number of transitions feeding into band 10 as well as on the configuration assignment for this sequence. The lowest spin state of band 12 is nearly degenerate with the $53/2^+$ level in band 10 (~ 20 keV), and the 764-keV link was determined to be of $E2$ character as its angular-correlation ratio was measured to be $R_{\text{ang}} = 1.03(6)$. All three of these bands are found to lie high in excitation energy relative to the other positive-parity structures in ^{167}Ta , as can be seen in Fig. 4(b). This indicates that they were likely populated at the highest spins and the intensity remained trapped in these sequences until lower spins were reached.

IV. DISCUSSION

Many proton orbitals are known to occur near the Fermi surface from recent work on high-spin states in $^{169,171,173}\text{Ta}$ [14–16]. These orbitals include the positive-parity $d_{3/2}[411]1/2$, $d_{5/2}[402]5/2$, $g_{7/2}[404]7/2$, and at higher energies $i_{13/2}[660]1/2$ states [17]. Commonly observed negative-parity orbitals include $h_{11/2}[514]9/2$ and $h_{9/2}[541]1/2$. By analyzing the alignment characteristics (including observed crossings) and the $B(M1)/B(E2)$ transition ratios (for the strongly coupled bands), configurations have been assigned for the bands, as discussed below. The alignments for the bands in ^{167}Ta are presented in Fig. 7 along with the ground-state band of ^{166}Hf , shown as the dashed line in this figure, for reference.

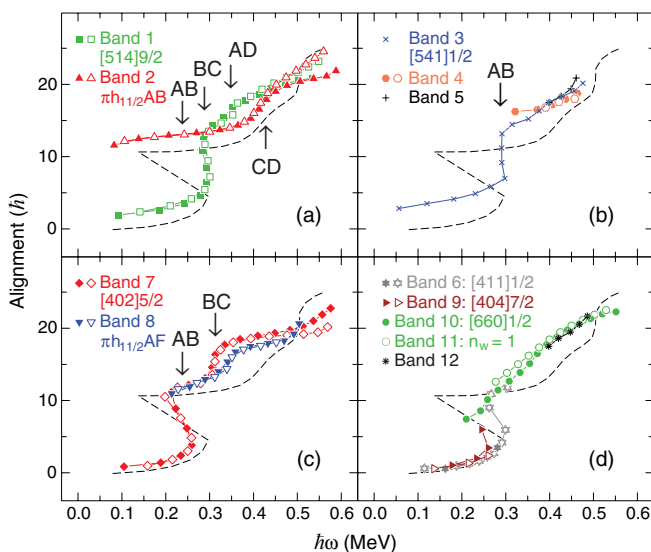


FIG. 7. (Color online) Alignments of the bands in ^{167}Ta plotted versus rotational energy $\hbar\omega$. Harris parameters of $\mathcal{J}_0 = 20 \hbar^2/\text{MeV}$ and $\mathcal{J}_1 = 40 \hbar^4/\text{MeV}^3$ were used to subtract the angular momentum of the rotating core. Observed crossings are designated in the figure. Solid (open) symbols denote the $\alpha = +1/2$ ($-1/2$) sequences. The dashed line represents the alignment observed in the ground-state band in ^{166}Hf .

TABLE II. Summary of configuration assignments and band crossing frequencies, $\hbar\omega_c$, observed in ^{167}Ta .

Band	Configuration ^a	$\hbar\omega_c$ (MeV)
1	$\pi h_{11/2} \rightarrow \pi h_{11/2}BC$	0.29
	$\pi h_{11/2}BC \rightarrow \pi h_{11/2}BCAD$	0.35
2	$\pi h_{11/2}AB \rightarrow \pi h_{11/2}ABCD$	0.41
3	$\pi h_{9/2} \rightarrow \pi h_{9/2}AB$	0.29
4	$(\pi d_{5/2}AEBC)$	
5	$(\pi d_{3/2}AEBC)$	
6	$\pi d_{3/2}$	
7	$\pi d_{5/2} \rightarrow \pi d_{5/2}AB$	0.24
	$\pi d_{5/2}AB \rightarrow \pi h_{11/2}AE$	> 0.24
	$\pi h_{11/2}AE \rightarrow \pi h_{11/2}AEBC$	0.31
8	$\pi h_{11/2}AF \rightarrow \pi h_{11/2}AFBC$	0.35
9	$\pi g_{7/2}$	
10	$\pi i_{13/2}$	
11	$\pi i_{13/2} n_w = 1$	
12	$(\pi i_{13/2})$	

^aTentative configurations are displayed in parentheses.

Harris parameters of $\mathcal{J}_0 = 20 \hbar^2/\text{MeV}$ and $\mathcal{J}_1 = 40 \hbar^4/\text{MeV}^3$ were selected to subtract the angular momentum of the core such that the ground-state band in ^{166}Hf [18] has nearly zero alignment at low frequencies, and nearly constant alignment following the first crossing. A summary of the configuration assignments and band crossing frequencies is provided in Table II.

A. Band 1: $\pi h_{11/2}[514]9/2$

The initial alignment of band 1 is approximately $1.5 \hbar$ more than that of the ground-state band in ^{166}Hf , as seen in Fig. 7(a). This value is consistent with the interpretation of the band being based on the $[514]9/2$ orbital, as suggested in Ref. [13]. Measured $B(M1)/B(E2)$ ratios for band 1 [Fig. 8(a)] are of similar values [~ 1 ($\mu_N/\text{eb})^2$] as those found in the $[514]9/2$ bands in the heavier isotopes $^{169,171}\text{Ta}$ [14, 15]. These experimental values are somewhat lower than those predicted when using the geometrical model $B(M1)$ estimate [19] with parameters of $g_R = Z/A = 0.44$, $g_\Omega = 1.30$, and the rotational form of $B(E2)$ [20] where the Q_0 moment was assumed to be 5.3 eb [21]. However, similar overestimations by theory were found in the heavier isotopes as well [14, 15]. Therefore, we are in agreement with Theine *et al.* [13] that band 1 is based on the $[514]9/2$ orbital of $h_{11/2}$ parentage.

Band 1 interacts with band 2 at a frequency of 0.24 MeV. This is a typical frequency for the AB crossing, where A and B refer to the lowest $i_{13/2}$ quasineutrons, as described in Sec. IV B. The continuation of the $[514]9/2$ sequence (band 1) persists up to a frequency of 0.29 MeV, where it encounters a different crossing. This is likely the BC crossing (alignment of the second- and third-lowest $i_{13/2}$ quasineutrons); however, its alignment gain of $\sim 9 \hbar$ is larger than expected. The crossing frequency is identical to the BC alignment observed in the odd-odd neighbors $^{166,168}\text{Ta}$ [22, 23], where only $7 \hbar$ of alignment was gained. A second crossing, with a large interaction strength, is found at a higher frequency, near 0.35 MeV, and has been attributed to the AD alignment based

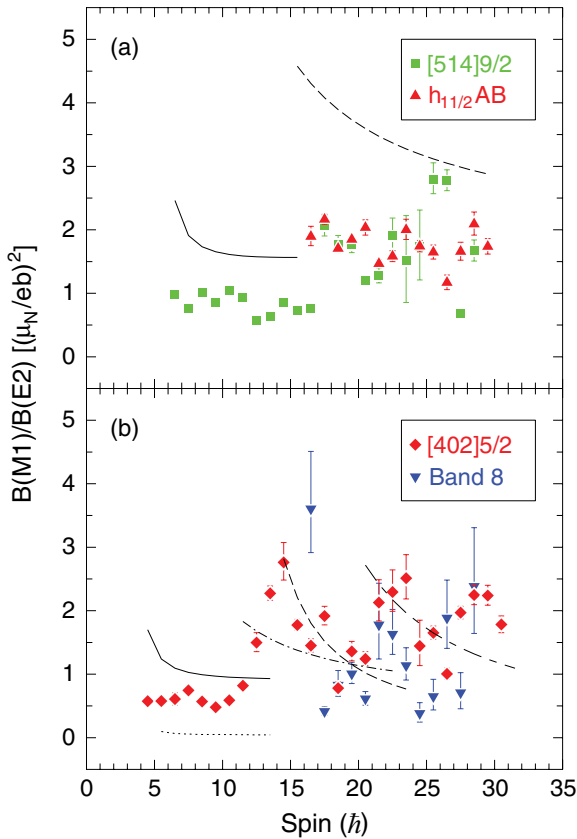


FIG. 8. (Color online) $B(M1)/B(E2)$ ratios for the bands denoted in the figure. In panel (a) the solid and dashed lines represent the theoretical values for the $[514]9/2$ and $\pi h_{11/2}AB$ configurations, respectively. In panel (b) the solid line denotes predicted ratios for the $[402]5/2$ band, while the dotted line is for the $[404]7/2$ configuration. The dash-dotted line refers to the $\pi d_{5/2}AB$ structure and the dashed line denotes the predicted values for the $\pi h_{11/2}AE$ band. Finally, the longdash-dotted line at high spins represents the theoretical ratios for the $\pi h_{11/2}AEB C$ configuration.

upon cranked shell model calculations similar to those shown in Refs. [15,23] that predict the AD crossing at 0.38 MeV.

The $B(M1)/B(E2)$ ratios are found to characteristically increase above spin $I = 33/2$ after the BC crossing, although the model again overestimates these values by a factor of two. It is interesting to note that the $B(M1)/B(E2)$ ratios for band 1 are nearly identical to those of band 2 above $I = 33/2$.

Above a frequency of 0.4 MeV, one may observe in Fig. 7(a) that the alignment of the signature partners of this $\pi h_{11/2}$ band split (with the favored $\alpha = -1/2$ sequence gaining more alignment), and this appears to be a general feature of this band throughout the $N \approx 96$ isotopes of thulium, lutetium, tantalum, and rhenium. The reason for this split is not at present clear, although some mixing with the unfavored signature of the $\pi h_{9/2}$ orbital at high frequency can perhaps be involved and cause the divergence of the signatures.

B. Band 2: $\pi h_{11/2}AB$ and band 2a

As seen in Fig. 7(a), band 2 parallels the ground-state band of ^{166}Hf , following the AB crossing while having $\sim 1.5\hbar$ more

alignment over most of the observed frequency range. For this reason, as well as the similarities of the $B(M1)/B(E2)$ ratios found between bands 1 and 2 in Fig. 8(a), we are in agreement with the $\pi h_{11/2}AB$ configuration assigned to band 2 in Ref. [13].

The BC and AD crossings found in band 1 are Pauli blocked in band 2; however, a crossing is observed at 0.41 MeV, just as in ^{166}Hf . This high-frequency crossing is associated with the CD alignment for ^{166}Hf [18], and the same interpretation is adopted here for the crossing in band 2. It is interesting to note that bands 1 and 2 consist of identical quasiparticles (an $h_{11/2}$ quasiproton coupled to four $i_{13/2}$ quasineutrons) above 0.4 MeV. One may see in Fig. 7(a) that their alignments are nearly identical above this frequency and that band 2 displays the same characteristic split of the $\pi h_{11/2}$ signatures. Also noted in this figure is that the crossing found near 0.5 MeV in ^{166}Hf is not observed in either bands 1 or 2. This observation strongly suggests that this high-frequency crossing in the even-even nucleus involves the $h_{11/2}$ quasiproton.

Band 2a may be associated with another $h_{11/2}$ orbital, but without further information, this is only a tentative assignment.

C. Band 3: $\pi h_{9/2}[541]1/2$

The large initial alignment ($\sim 3\hbar$) and the absence of a signature partner indicate that band 3 is based on a low- K member of a high- j shell. Furthermore, band 3 was determined to have negative parity; therefore, only the $[541]1/2$ orbital which is near the Fermi surface can satisfy these characteristics. A crossing is found just below a frequency of 0.3 MeV and it is interpreted as the AB alignment. This crossing frequency is delayed with respect to the AB crossings found in ^{166}Hf , but this is a well-documented trait for bands built on the $h_{9/2}$ orbital [24]. Above 0.35 MeV, the alignment appears to continue to increase; this may be associated with the CD crossing or may result from an improper choice of Harris parameters as the band is based on an orbital known to drive the nucleus to higher deformation (see Ref. [24] and references therein).

D. Bands 4 and 5

These structures, which are most likely of negative parity, are analogous to sequences observed in the neighboring isotope ^{165}Lu [25]. Multiple coupled bands were observed to interact with the $\pi h_{11/2}$ configuration at high spin in ^{165}Lu and were assigned configurations of $\pi h_{11/2}BC$ (corresponding to band 1 in ^{167}Ta) and $\pi g_{7/2}AE$ (where E represents the lowest negative parity, $\alpha = +1/2$ quasineutron orbital). As the Fermi surface is closer to the $\pi d_{5/2}$ orbital in ^{167}Ta , band 4 is more likely associated with the $\pi d_{5/2}AE$ configuration after it has experienced the BC crossing. Such a configuration would have an alignment similar to (but slightly smaller than) band 7 above 0.31 MeV (where a configuration of $\pi h_{11/2}AEB C$ has been assigned; see Sec. IV F). This is, indeed, observed as a comparison can be made between the two bands in Figs. 7(b) and 7(c). However, this assignment must be regarded as tentative without further experimental confirmation of the parity.

A decoupled sequence feeding into the $\pi h_{9/2}$ band at 45/2 is found in ^{165}Lu that is similar to band 5 in ^{167}Ta . No configuration was suggested in Ref. [25] as it is difficult to propose an assignment with little information about the structure. Perhaps this corresponds to the $\pi d_{3/2}AEBC$ sequence, as such a configuration would have approximately the same alignment as band 4. Once again, this assignment must be regarded as tentative, pending further experimental information.

E. Band 6: $\pi d_{3/2}[411]1/2$

Band 6 displays nearly no initial alignment [Fig. 7(d)] and exhibits significant signature splitting (Fig. 2). These characteristics are consistent with a low- K orbital from a low- j shell. Thus, band 6 has been assigned the $[411]1/2$ configuration. Only two reliable $B(M1)/B(E2)$ ratios could be determined and their value was found to be quite low [$\sim 0.1 (\mu_N/\text{eb})^2$], which is consistent with the predicted value $[0.08 (\mu_N/\text{eb})^2]$ using the same parameters as discussed for band 1 except $g_\Omega = -1.10$. A crossing is observed in the favored $\alpha = -1/2$ signature at 0.28 MeV. This crossing frequency is closer to the BC alignment than to the AB alignment. It is possible that this is a delayed AB crossing, similar to that observed in the $[541]1/2$ band, but no such delays have ever been observed in the $[411]1/2$ bands of the neighboring nuclei. Perhaps the AB crossing is affected by another three-quasiparticle band that disturbs the expected crossing frequency. Indeed, such a band is found to cross the $[411]1/2$ configuration in this same frequency region in the nearby nucleus ^{171}Re [26]. Further experimentation is required to fully account for this unusual feature.

F. Band 7: $\pi d_{5/2}[402]5/2$

This strongly coupled sequence has a small amount of initial alignment [Fig. 7(c)], indicating that it is likely based on a high- K member of its shell. As this band very likely has positive parity, the $[402]5/2$ and $[404]7/2$ orbitals are both possible configurations. In Fig. 8(b), one finds that the experimental $B(M1)/B(E2)$ values lie between those predicted for the $[402]5/2$ orbital (solid line) and the $[404]7/2$ one (dotted line). The large difference between the two orbitals is a result of their different g_Ω values: 1.57 for $[402]5/2$ and 0.61 for $[404]7/2$. A similar result was found in ^{169}Ta [14] and this indicates that a large amount of mixing of these two configurations is present in band 7. This is further confirmed by the number of interband transitions between bands 7 and 9 (Fig. 2). The $B(M1)/B(E2)$ ratios slightly favor the $[402]5/2$ assignment, and Fig. 13 in Ref. [14] indicates that there is a trend of the $[404]7/2$ state lying above the $[402]5/2$ one. Therefore, we are in agreement with Ref. [13] that band 7 is predominantly based on the $[402]5/2$ orbital.

At a frequency of 0.24 MeV, a large alignment gain occurs in band 7 [see Fig. 7(c)]. It can be attributed to the AB crossing. A second crossing is observed at 0.31 MeV, which is consistent with the BC crossing observed in band 1. However, the BC alignment would not be allowed in band 7, if it is associated with the $\pi d_{5/2}AB$ configuration. Similar

observations have been reported in the $[404]7/2$ bands of ^{171}Ta [15] and $^{163,165}\text{Lu}$ [25,27]. In Ref. [27], Jensen *et al.* first suggested that the positive-parity band is crossed by a three-quasiparticle band consisting of an $h_{11/2}$ quasiproton with an $i_{13/2}$ and an $h_{9/2}$ quasineutron ($\pi h_{11/2}AE$) during or just after the AB alignment. This scenario allows for the BC crossing. The $B(M1)/B(E2)$ ratios extracted above the first crossing, shown in Fig. 8(b), do provide evidence for this change of configuration in band 7. Between spins 29/2 and 41/2, the $B(M1)/B(E2)$ values fall from nearly $3 (\mu_N/\text{eb})^2$ to $1 (\mu_N/\text{eb})^2$. The dashed-dotted line in Fig. 8(b) refers to the predicted values, assuming a $\pi d_{5/2}AB$ configuration, while the dashed line refers to the calculated ratios for the $\pi h_{11/2}AE$ configuration. Clearly the latter calculations reproduce the data better. Above $I = 41/2$, the BC alignment occurs, and good reproduction of the experimental $B(M1)/B(E2)$ data is achieved with the theoretical ratios, assuming the $\pi h_{11/2}AEBC$ configuration. In addition, one may note the splitting in the alignment plot of band 7 above 0.4 MeV which is characteristic of the presence of an $h_{11/2}$ quasiproton in the configuration.

G. Band 8: $\pi h_{11/2}AF$

Band 8 is likely based on a three-quasiparticle configuration owing to the fact that it is not observed until an excitation energy of over 3 MeV is reached. This structure strongly interacts with band 7 after the crossing with the $\pi h_{11/2}AE$ configuration. The presence of numerous interactions may indicate that the two bands are based on similar intrinsic structures, that is with an $h_{11/2}$ quasiproton coupled to an $i_{13/2}$ and an $h_{9/2}$ quasineutron. Note that the measured $B(M1)/B(E2)$ ratios [Fig. 8(b)] are quite scattered, but they are similar to band 7 in this spin region. The alignment for bands 7 and 8 are also nearly identical below 0.3 MeV, as seen in Fig. 7(c). A crossing is observed in band 8 at 0.35 MeV, a frequency slightly higher than that for the BC alignment in band 7. This may suggest that the alignment in band 8 is associated with the AD crossing, which would imply a $\pi h_{11/2}BE$ configuration. However, the B quasineutron is known to lie much higher in energy than the A quasineutron. In Fig. 4(b), band 8 lies only slightly higher than band 7, so the $\pi h_{11/2}BE$ configuration does not seem to be a satisfactory assignment for band 8, although it cannot be completely ruled out. Instead, a $\pi h_{11/2}AF$ configuration is favored, where the BC alignment is delayed. In fact the BC crossings are found to differ slightly in the AE and AF bands observed in ^{166}Hf [18] and ^{168}W [28] as well.

H. Band 9: $\pi g_{7/2}[404]7/2$

This short, coupled sequence of transitions has nearly zero initial alignment [Fig. 7(d)] and there are several linking γ rays between the $[402]5/2$ sequence and this structure. The $B(M1)/B(E2)$ ratios were found to be small, on the order of $0.2 (\mu_N/\text{eb})^2$, which is consistent with the predicted value of $0.1 (\mu_N/\text{eb})^2$ at the lowest spins of the $[404]7/2$ band. Therefore, band 9 is assigned as the structure based upon the $[404]7/2$ orbital of $g_{7/2}$ parentage.

I. Bands 10, 11, and 12: Sequences based on $\pi i_{13/2}[660]1/2$

These three decoupled structures were the focus of our recent article [4], where arguments were presented associating band 10 with the $[660]1/2$ orbital and, more importantly, band 11 with the $n_w = 1$ wobbling partner, built on this $\pi i_{13/2}$ configuration. One of the key signatures for the identification of a wobbling sequence is that its characteristics are identical to those of the $i_{13/2}$ band (most notably its alignment and dynamic moment of inertia). The similarity of alignments between bands 10 and 11 is clearly visible in Fig. 7(d) for frequencies above $\hbar\omega \approx 0.35$ MeV. However, below this frequency there is a difference of $\sim 1 \hbar$. As discussed in Ref. [4], the lower-spin portion of band 10 may be based on the $i_{13/2}$ quasiproton in an axially symmetric minimum, and the gain of $1 \hbar$ of alignment near 0.35 MeV is a result of the transition into the TSD minimum. With this interpretation, band 12 may then be considered as the continuation of the $[660]1/2$ structure in the axially symmetric minimum.

V. DECREASING WOBBLING PHONON ENERGY

Although the first description of the collective wobbling mode was based on even-even nuclei, all examples available to date have been observed in odd- A systems. In fact, the unpaired, highly aligned $i_{13/2}$ quasiproton has proven to play a pivotal role in the observation of wobbling in lutetium and tantalum nuclei. As first suggested in Ref. [5], the $i_{13/2}$ quasiproton drives the nuclear shape toward a larger deformation than the other quasiparticle states located near the Fermi surface. At these larger deformations, a significant gap in the quasineutron energy levels opens at $N = 94$ and stabilizes an asymmetric shape with $\gamma \approx 20^\circ$.

Following the initial discovery of the first wobbling structure in ^{163}Lu [1], particle-rotor model calculations were primarily used to describe features of this exotic wobbling mode (see Refs. [29–31]). Random-phase approximation calculations were also able to reproduce experimental results of the wobbling bands (see Refs. [32–35]). In particular, the unusually large transition strength ratios $B(E2)_{\text{out}}/B(E2)_{\text{in}}$ could be described within both models. However, this particle-rotor model description of the wobbling energy assuming constant moments of inertia has not been able to reproduce a systematic feature seen in all the known wobbling bands and is described below.

Figure 9 displays the energy associated with the $n_w = 1$ wobbling phonon in the five cases where this phenomenon has been observed. The wobbling energy is calculated as

$$\hbar\omega_w = E_1(I) - [E_0(I+1) + E_0(I-1)]/2, \quad (1)$$

where $E_1(I)$ is the energy of the state with spin I in the $n_w = 1$ wobbling band, and E_0 the energy of the state in the $\pi i_{13/2}$ band. The magnitude of the wobbling phonon energy is similar in each case. A clear trend of decreasing energy with spin (that is nearly linear, with the exception of ^{161}Lu) is observed, where the slopes are nearly identical for $^{163},^{165}\text{Lu}$ and ^{167}Ta above spin 51/2. The two slopes found in ^{167}Ta may be a result of the $\pi i_{13/2}$ structure lying in a $\gamma \approx 0^\circ$ minimum below $I = 51/2$, while lying in a TSD minimum above this

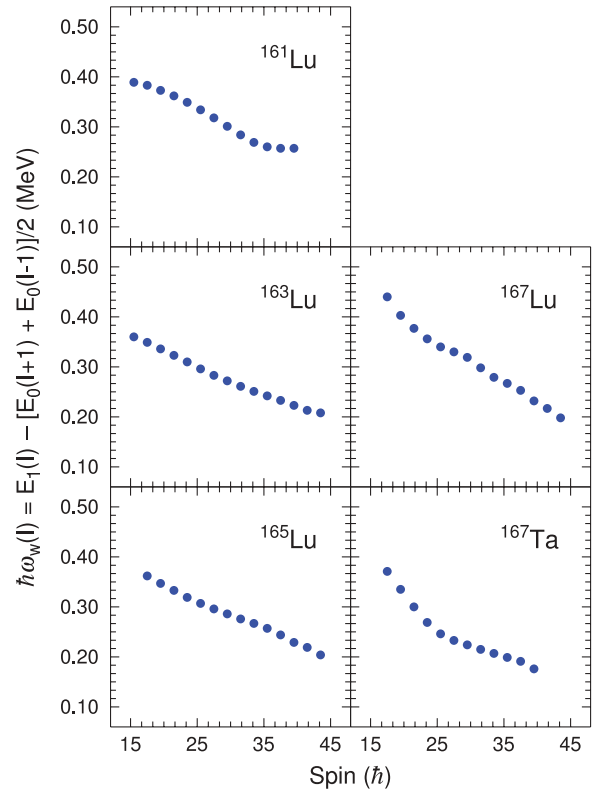


FIG. 9. (Color online) Wobbling phonon energy ($\hbar\omega_w$), as described in the text, versus spin for the five known cases of wobbling in lutetium and tantalum nuclei.

spin, as alluded to above and as discussed in Ref. [4]. In ^{167}Lu , a slightly steeper slope is observed, which is even more pronounced at the lowest spins. This may be an indication of an evolution from a symmetric to an asymmetric minimum, as in ^{167}Ta .

The importance of the aligned $i_{13/2}$ quasiproton for wobbling has been discussed in the publications noted above and the relevant Hamiltonian has been given in several references (e.g., Refs. [30,31,36,37]). The inherent problem with this Hamiltonian, in regards to the experimental results of Fig. 9, is best displayed in Fig. 12 of Ref. [31]. There one may observe that the Hamiltonian suggests that the wobbling energy should increase linearly with spin, which is opposite to the experimental findings (Fig. 9). In Refs. [36,37], Tanabe and Sugawara-Tanabe considered whether a spin-dependent moment of inertia may be able to better reproduce the energy levels of the $\pi i_{13/2}$ bands and the wobbling sequences associated with them. Their justification for this approach is based upon the fact that the observed increase in dynamic moment of inertia with frequency suggests a decrease in pairing with spin. By replacing the moment of inertia with a spin-dependent value of

$$\mathcal{J}_0 \rightarrow \mathcal{J}_0 \frac{I - c_1}{I + c_2}, \quad (2)$$

constants were chosen to model the decreasing wobbling energy, with $c_1 = 0.69$, $c_2 = 23.5$, and $\mathcal{J}_0 = 77.6 \text{ MeV}^{-1}$ selected for ^{163}Lu . Specifically, one can then infer a slight

decrease of the wobbling energy for $^{161,163,165,167}\text{Lu}$ in Figs. 5, 6, 7, and 8 of Ref. [36]. With these parameters the transition strength ratios were also satisfactorily reproduced within the model. Similar results are displayed for ^{167}Ta in Ref. [37], but different parameters were utilized in Eq. (2). It is possible to gauge the effectiveness of these angular momentum dependent moments of inertia by scaling the wobbling frequency with the inverse of the moment of inertia. From Fig. 12 in Ref. [31], the ratio of the wobbling frequencies at spin $I = 40$ and 17 is found to be $\hbar\omega(I = 40)/\hbar\omega(I = 17) \approx 1.2$, but this work assumed constant moments of inertia. Using Eq. (2) gives a ratio of the moments of inertia of $\mathcal{J}_0(I = 40)/\mathcal{J}_0(I = 17) = 1.54$ between the same spin values. This produces a scaled ratio of the wobbling frequency equal to $1.2/1.54 = 0.78$ that is close to the experimental ratio $\hbar\omega(I = 40)/\hbar\omega(I = 17) = 0.63$, determined from the ^{163}Lu data displayed in Fig. 9. However, the remaining difference between these ratios leads to the conclusion that the observed decrease in wobbling energy cannot be fully explained by an increase in the moments of inertia resulting from the attenuation of pair correlations. In addition, the calculated moments of inertia using Eq. (2) and the parameters defined above are low in the $I = 17\text{--}40$ spin range (between 30 and 50 MeV^{-1}) in comparison with the experimental values within the same range (between 62 and 75 MeV^{-1}).

An alternative approach, using random-phase calculations [32–34], has also attempted to explain the decreasing wobbling energy with spin. With this microscopic method, a nearly constant wobbling energy was calculated for ^{163}Lu (see Fig. 2 in Ref. [32]) and a decrease was even found at the highest frequencies. However, the wobbling energy was underestimated by nearly a factor of two at the lower frequencies, and predictions of the transition strength ratios were not nearly as satisfactory as those found using particle-rotor model methods. Shoji and Shimizu [38] performed random-phase calculations based on a Woods-Saxon potential (rather than a Nilsson potential as in Refs. [32–34]) and were able to calculate a decreasing wobbling frequency for ^{163}Lu . Once again, however, the wobbling frequency was significantly

underestimated as seen in Fig. 6 of Ref. [38], although the transition strength ratios were reproduced quite well in comparison to the experimentally determined values. From the discussion above, it is therefore concluded that, even though theoretical progress has been made, a complete description of the wobbling phenomenon in the lutetium/tantalum region remains a challenge that requires further investigation.

VI. SUMMARY

More than 370 transitions and 12 bands are now known in the $N = 94$ nucleus ^{167}Ta . All four (AB , BC , AD , CD) crossings based on $i_{13/2}$ quasineutrons were observed, and these crossings helped to assign configurations to the structures. The $\pi i_{13/2}$ sequence was confirmed and a structure that is likely based on the $n_w = 1$ wobbling phonon was observed. The energy associated with this phonon is found to decrease with energy in a manner similar to that observed previously in wobbling bands of $^{163,165,167}\text{Lu}$. The decrease is nearly linear and is opposite to the predictions of the particle-rotor model when constant moments of inertia are assumed. While progress has been made to theoretically understand the wobbling mode using particle-rotor and random-phase approximation models, a comprehensive explanation for this phenomenon is needed and will be a challenge to the theoretical community.

ACKNOWLEDGMENTS

The authors thank the ANL operations staff at Gammasphere and gratefully acknowledge the efforts of J. P. Greene for target preparation. We thank D. C. Radford and H. Q. Jin for their software support. This work is funded by the National Science Foundation under Grants No. PHY-0854815 (USNA), No. PHY-0754674 (FSU), and No. PHY07-58100 (ND), as well as by the US Department of Energy, Office of Nuclear Physics, under Contract No. DE-AC02-06CH11357 (ANL), and Grants No. DE-FG02-94ER40848 (UML), No. DE-FG02-94ER40834 (UM), No. DE-FG02-95ER40939 (MSU), and No. DE-FG02-96ER40983 (UT).

-
- [1] S. W. Ødegård *et al.*, *Phys. Rev. Lett.* **86**, 5866 (2001).
 - [2] G. Schönwaßer *et al.*, *Phys. Lett. B* **552**, 9 (2003).
 - [3] N. S. Pattabiraman *et al.*, *Phys. Lett. B* **647**, 243 (2007).
 - [4] D. J. Hartley *et al.*, *Phys. Rev. C* **80**, 041304(R) (2009).
 - [5] H. Schnack-Petersen *et al.*, *Nucl. Phys. A* **594**, 175 (1995).
 - [6] P. Bringel *et al.*, *Eur. Phys. J. A* **24**, 167 (2005).
 - [7] H. Amro *et al.*, *Phys. Lett. B* **553**, 197 (2003).
 - [8] R. V. F. Janssens and F. S. Stephens, *Nucl. Phys. News* **6**, 9 (1996).
 - [9] I.-Y. Lee, *Nucl. Phys. A* **520**, 641c (1990).
 - [10] M. Cromaz, T. J. M. Symons, G. J. Lane, I. Y. Lee, and R. W. MacLeod, *Nucl. Instrum. Methods Phys. Res., Sect. A* **462**, 519 (2001).
 - [11] D. C. Radford, *Nucl. Instrum. Methods Phys. Res., Sect. A* **361**, 297 (1995).
 - [12] F. Meissner, W.-D. Schmidt-Ott, V. Freystein, T. Hild, E. Runte, H. Salewski, and R. Michaelsen, *Z. Phys. A* **332**, 153 (1989).
 - [13] K. Theine *et al.*, *Nucl. Phys. A* **536**, 418 (1992).
 - [14] D. J. Hartley *et al.*, *Phys. Rev. C* **74**, 054314 (2006).
 - [15] D. J. Hartley *et al.*, *Phys. Rev. C* **72**, 064325 (2005).
 - [16] H. Carlsson *et al.*, *Nucl. Phys. A* **592**, 89 (1995).
 - [17] W. Nazarewicz, M. A. Riley, and J. D. Garrett, *Nucl. Phys. A* **512**, 61 (1990).
 - [18] D. Ringkjøbing Jensen *et al.*, *Eur. Phys. J. A* **8**, 165 (2000).
 - [19] F. Dönau, *Nucl. Phys. A* **471**, 469 (1987).
 - [20] A. Bohr and B. R. Mottelson, *Nuclear Structure*, Vol. II (Benjamin, New York, 1975).
 - [21] P. Möller, J. R. Nix, W. D. Myers, and W. J. Swiatecki, *At. Data Nucl. Data Tables* **59**, 185 (1995).

- [22] D. J. Hartley *et al.*, *Phys. Rev. C* **82**, 057302 (2010).
- [23] X. Wang *et al.*, *Phys. Rev. C* **82**, 034315 (2010).
- [24] H. J. Jensen *et al.*, *Nucl. Phys. A* **695**, 3 (2001).
- [25] G. Schönwaßer *et al.*, *Nucl. Phys. A* **735**, 393 (2004).
- [26] D. J. Hartley *et al.* (unpublished).
- [27] D. R. Jensen *et al.*, *Nucl. Phys. A* **703**, 3 (2002).
- [28] K. Theine *et al.*, *Nucl. Phys. A* **548**, 71 (1992).
- [29] I. Hamamoto, *Phys. Rev. C* **65**, 044305 (2002).
- [30] I. Hamamoto and G. B. Hagemann, *Phys. Rev. C* **67**, 014319 (2003).
- [31] K. Tanabe and K. Sugawara-Tanabe, *Phys. Rev. C* **73**, 034305 (2006).
- [32] M. Matsuzaki, Y. R. Shimizu, and K. Matsuyanagi, *Phys. Rev. C* **65**, 041303(R) (2002).
- [33] M. Matsuzaki, Y. R. Shimizu, and K. Matsuyanagi, *Phys. Rev. C* **69**, 034325 (2004).
- [34] Y. R. Shimizu, T. Shoji, and M. Matsuzaki, *Phys. Rev. C* **77**, 024319 (2008).
- [35] M. Oi, *Phys. At. Nucl.* **70**, 1577 (2007).
- [36] K. Tanabe and K. Sugawara-Tanabe, *Phys. Rev. C* **77**, 064318 (2008).
- [37] K. Sugawara-Tanabe and K. Tanabe, *Phys. Rev. C* **82**, 051303(R) (2010).
- [38] T. Shoji and Y. Shimizu, *Int. J. Mod. Phys. E* **15**, 1407 (2006).